Film structure

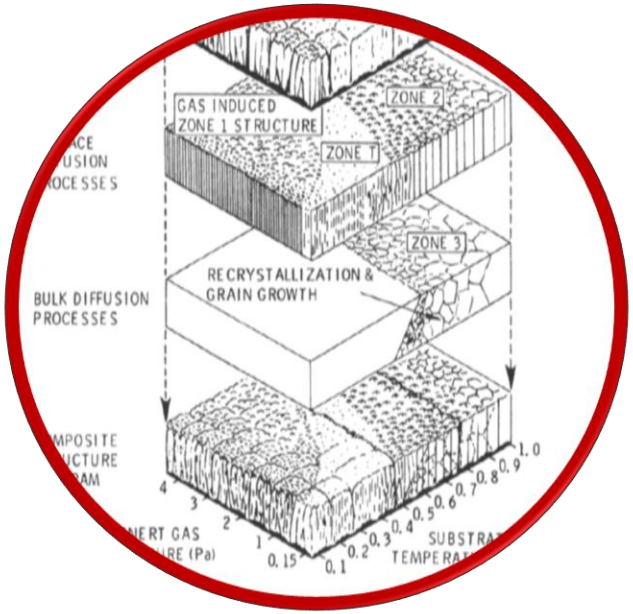

content

- Evaporated & sputtered films: shadowing, surface and bulk diffusion, desorption
- Structure –Zone – Model (SZM) diagram for evaporation
- SZM for sputtered films: Temperature and pressure
- SZM for ion bombardment
- Columnar grain morphology
- Columnar grains – tangent rule & nested columnar microstructure
- Film density
- Results from Monte-Carlo and MD simulations – zone I
- Grain growth – parabolic time dependence
- Grain growth – abnormal growth and texture
- Energetics of grain growth
- Texture:
  - effect of temperature, strain, thickness, substrate, ion bombardment, surface patterning
  - role of diffraction methods
  - Stages of texture evolution
  - Temperature effect in detail
  - Strain energy vs surface energy
- Sculptured films
- Amorphous thin films

Structure zone models for evaporated and sputtered films

Structural morphologies of metal, semiconductor, and ceramic films possess similar features

Condensation from the vapor involves **incident atoms becoming bonded adatoms** which then **diffuse over the film surface until they desorb or, more commonly, are trapped at low-energy lattice sites**.

Finally, **incorporated atoms** reach their **equilibrium position in the lattice** by bulk diffusive motion. This atomic odyssey involves four basic processes:

(1) shadowing,
(2) surface diffusion,
(3) bulk diffusion,
(4) desorption.

The **last three** are quantified by the characteristic diffusion and sublimation activation energies whose magnitudes **scale directly with the melting point TM of the condensate**.

Shadowing is a phenomenon arising from the **geometric constraint** imposed by the roughness of the growing film and the line-of-sight impingement of arriving atoms.

The **dominance of one or more** of these four processes as a function of substrate temperature, Ts, is manifested by different structural morphologies. This is the basis of **structure-zone models (SZMs)**, which have been devised to characterize film and coating grain structures.

SZM diagram for evaporated films

The structures were identified as belonging to one of three zones (1, 2, 3) based on the ratio T_S/T_M:

Zone 1 structures **(T_S/T_M < 0.3)** are columnar, consisting of inverted conelike units capped by domes and separated by voided boundaries.They arise from **shadowing effects** and **frozen** or **very limited adatom motion**.

The **zone 2** structure **(0.3 < T_S/T_M < 0.50)** is also columnar but with tighter metallurgical grain boundaries that are ~0.5 nm wide. Surface or grain-boundary diffusion apparently plays a role in the evolution of this structure, because the columnar grain size increases with T_S/T_M in accord with the activation energies for these mass-transport mechanisms.

Equiaxed grains that grow in size by bulk diffusion characterize **zone 3** structures **(T_S/T_M > 0.5)**.

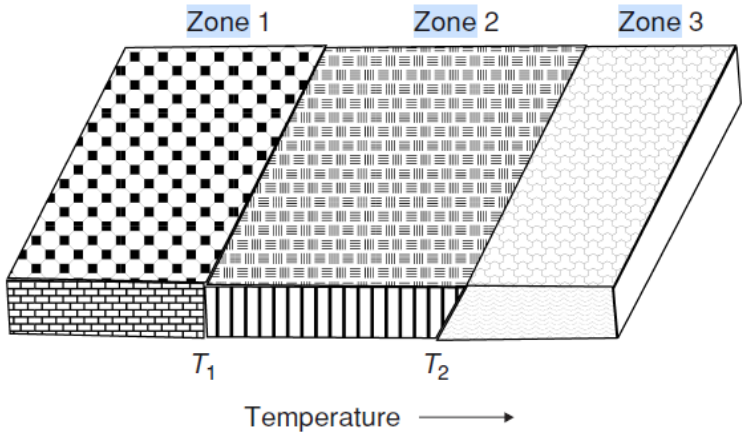

Mattox 2010
Harsha 2010

Thornton diagram for sputtered films

A similar zone scheme was introduced by **Thornton for sputtered metal** deposits but with four zones (1, T, 2, 3). Thornton introduced a T-zone to represent the transition zone from zone I to zone II microstructure.

The exploded view illustrates the effect of the individual physical processes on structure and how they depend on **substrate temperature**, the ever-present variable, and **inert sputtering gas pressure (P)**.

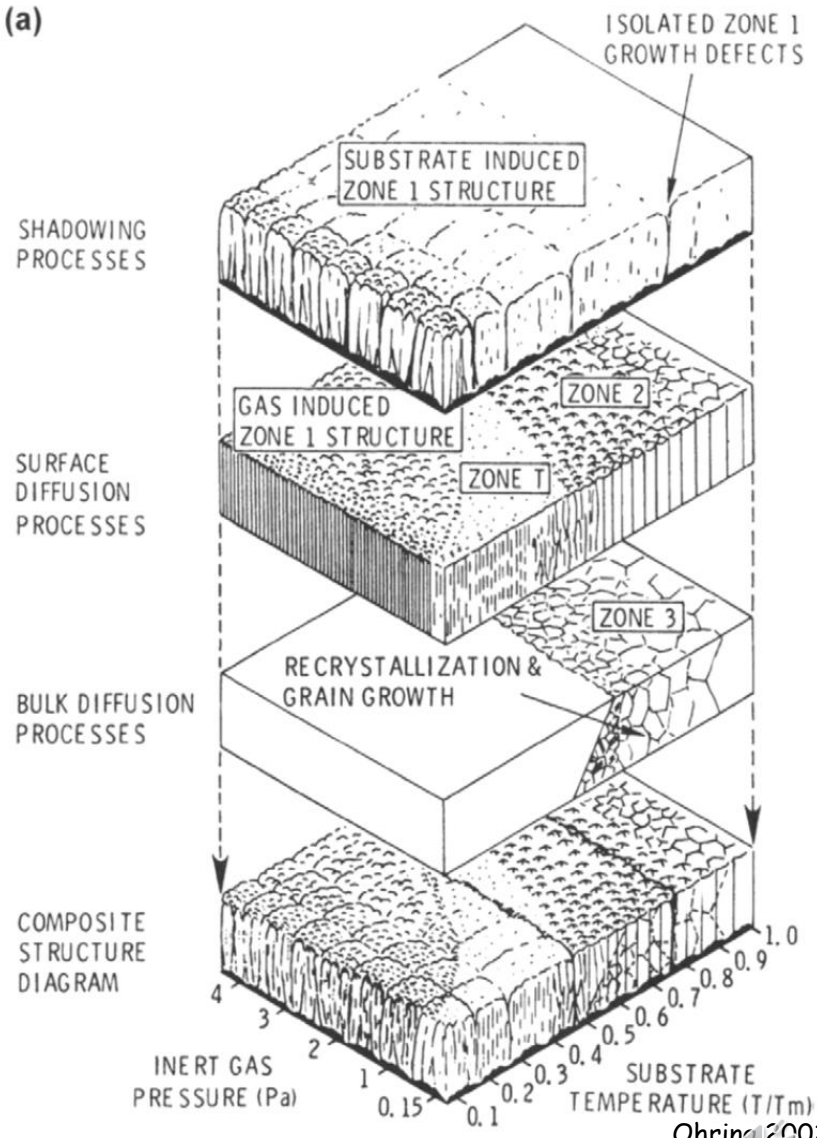

Thornton diagram for sputtered films

Pressure affects film microstructure through several indirect mechanisms.

For example, if **the pressure is increased** to the point where the mean free path for elastic collisions between the sputtered atoms and sputtering gas becomes of the order of the source-substrate distance, the oblique component of the deposition flux is increased because of gas scattering; this results in a more open zone 1 structure.

On the other hand, a **reduction in gas pressure** results in increased energetic-particle bombardment which in turn densities the film.

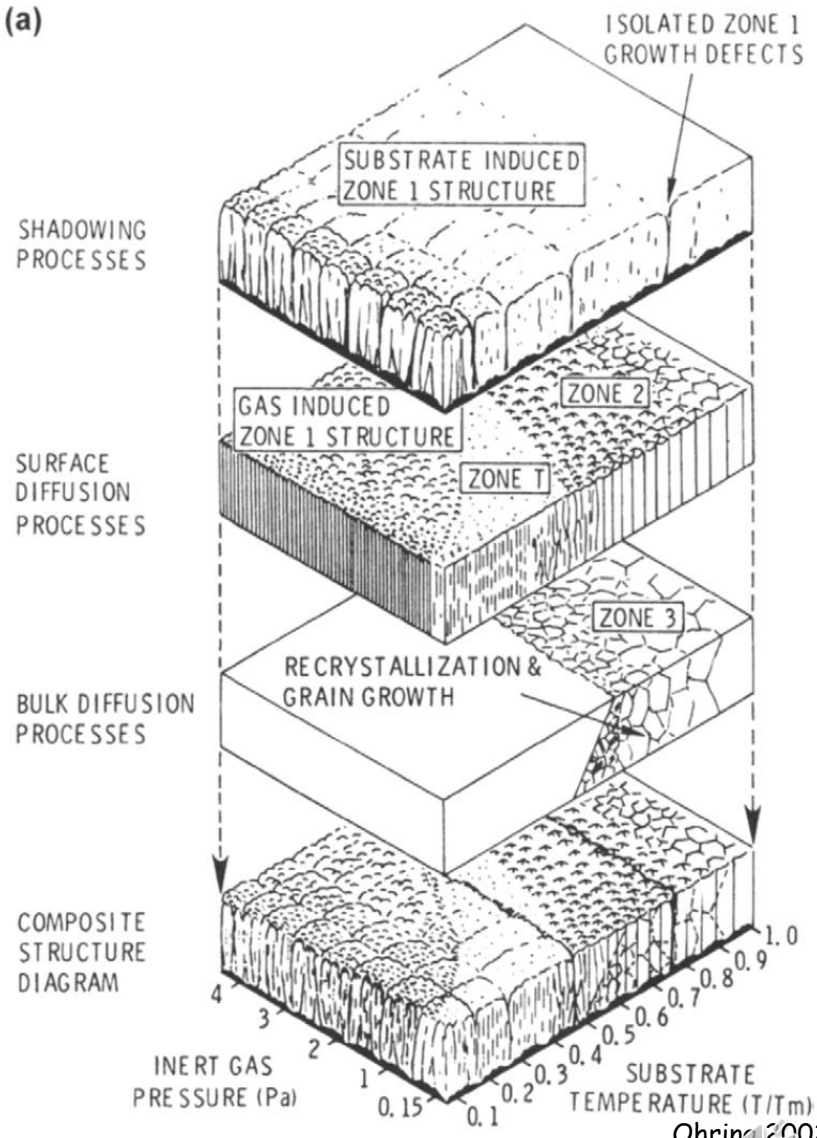

Ohring 2002

Structure zone models for ion beam bombardment

This SZD for **ion bombardment** differs from that presented for sputtering because the floating **bias potential** at the substrate (Vs) replaces pressure (P) as a variable.

We note, however, that **raising Vs enhances the extent of ion bombardment**, a situation that can also be accomplished by **reducing P**. Thus Vs varies inversely with P and we may expect some distortion in the zone 1/zone T domains .

Specifically, zone T is widened relative to zone 1 because **ion bombardment promotes adatom motion** and therefore has the same **effect as raising substrate temperatures**.

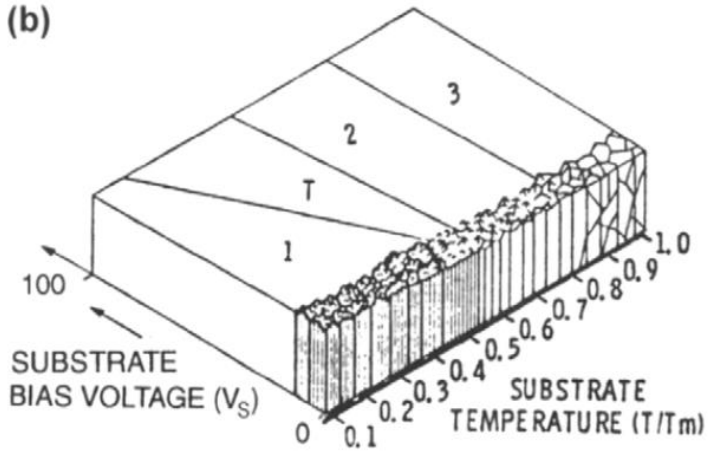

Zone structures in thick evaporated and sputtered coatings

Zone	T_S/T_M	Structural characteristics	Film properties
1(E)	<0.3	Tapered crystals, dome tops, voided boundaries.	High dislocation density, hard.
1(S)	<0.1 at 0.15 Pa to <0.5 at 4 Pa	Voided boundaries, fibrous grains. Zone 1 is promoted by substrate roughness and oblique deposition.	Hard.
T(S)	0.1–0.4 at 0.15 Pa, 0.4–0.5 at 4 Pa	Fibrous grains, dense grain boundary arrays.	High dislocation density, hard. High strength, low ductility.
2(E)	0.3–0.5	Columnar grains, dense grain boundaries.	Hard, low ductility.
2(S)	0.4–0.7		
3(E)	0.5–1.0	Large equiaxed grains, bright surface.	Low dislocation density, soft recrystallized grains.
3(S)	0.6–1.0		

columnar (grain) morphology

columnar structures are observed when the **mobility of deposited atoms is limited** and therefore their occurrence is ubiquitous.

For example, columnar grains have been observed **in high melting point materials** (Cr, Be, Si, and Ge), in compounds of **high binding energy** (TiC, TiN, CaF_2, and PbS), and in **nonnoble metals evaporated in the presence of oxygen** (Fe and Fe-Ni).

Amorphous films of Si, Ge, SiO, and rare earth-transition metal alloys (e.g., Gd-Co) whose very existence depends on limited adatom mobility **are frequently columnar** when deposited at sufficiently low temperatures.

As grain boundaries are axiomatically absent in amorphous films, it is perhaps more correct to speak of **columnar morphology** in this case. This columnar morphology is frequently made visible by **transverse fracture** of the film because of crack propagation along the weak, low-density intercolumnar regions.

Magnetic, optical, electrical, mechanical, and **surface properties** of films are affected, sometimes strongly, by columnar structures.

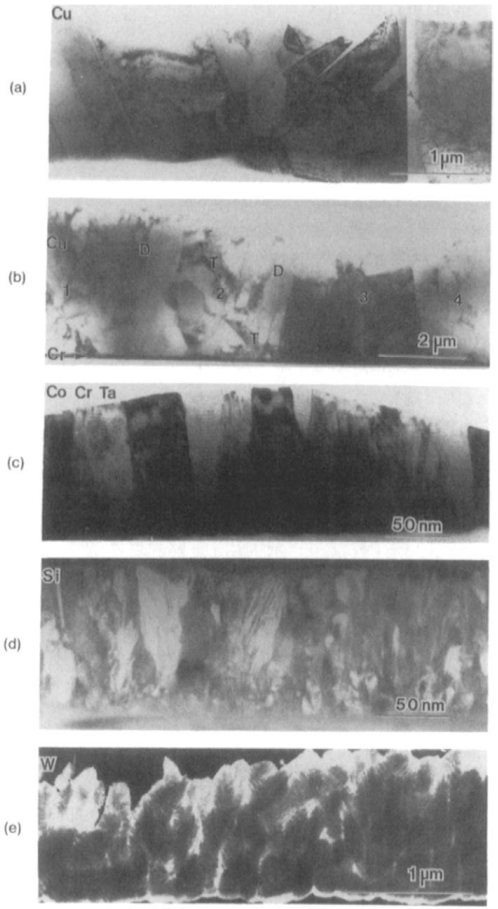

Figure 9-4 Representative set of cross-sectional transmission electron micrographs of thin films illustrating variants of columnar microstructures. (a) Acid-plated Cu, (b) sputtered Cu, (c) sputtered Co–Gd–Ta alloy, (d) CVD silicon (also Fig. 6-23), (e) sputtered W. D = dislocation, T = twin. (Courtesy of D. A. Smith, IBM, T. J. Watson Research Center. From M. F. Chisholm and D. A. Smith, in *Advanced Techniques for Microstructural Characterization*, eds. R. Krishnan, T. R. Anantharaman, C. S. Pande, and O. P. Arora, Trans-Tech Publications, Switzerland, 1988. Reprinted with permission from Trans-Tech Publications.)

columnar grains – tangent rule

An interesting observation on the geometry of columnar grains has been formulated as the so-called **Tangent Rule**.

Careful measurements on obliquely evaporated films reveal that the columns are **oriented toward the vapor source** .

By varying the incident vapor angle over a broad range it was experimentally found that the relation holds:

$$\tan \alpha = 2 \tan \beta.$$

The very general occurrence of the columnar morphology implies a simple nonspecific origin such as geometric shadowing

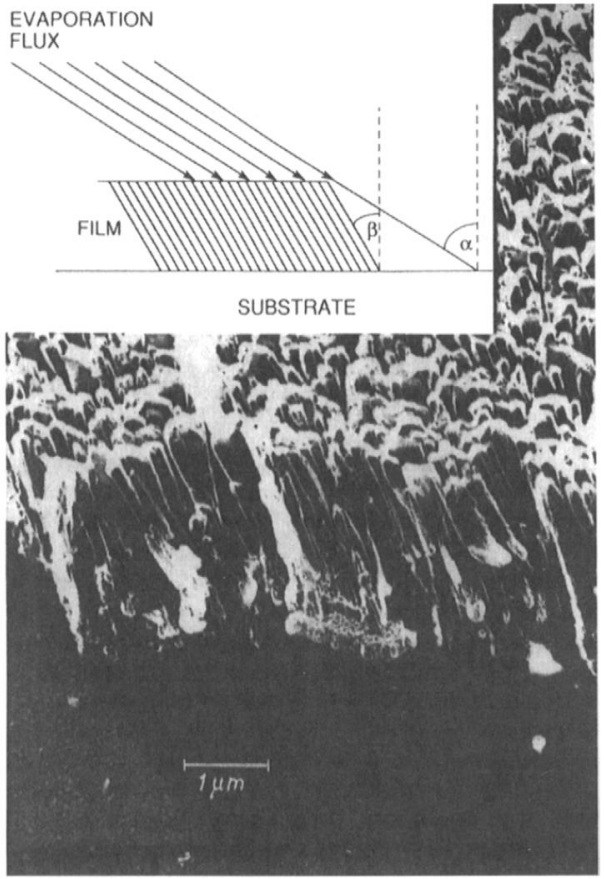

Figure 9-5 Electron micrograph of a replica of a 1 μm thick Al film (Ref. 12). Inset shows deposition geometry that leads to the Tangent Rule.

Nested nano-, micro-, and macrocolumns,

When prepared under low adatom mobility conditions (Ts/TM < 0.5), three general structural units are recognized; nano-, micro-, and macrocolumns, together with associated nano-, micro-, and macrovoid distributions.

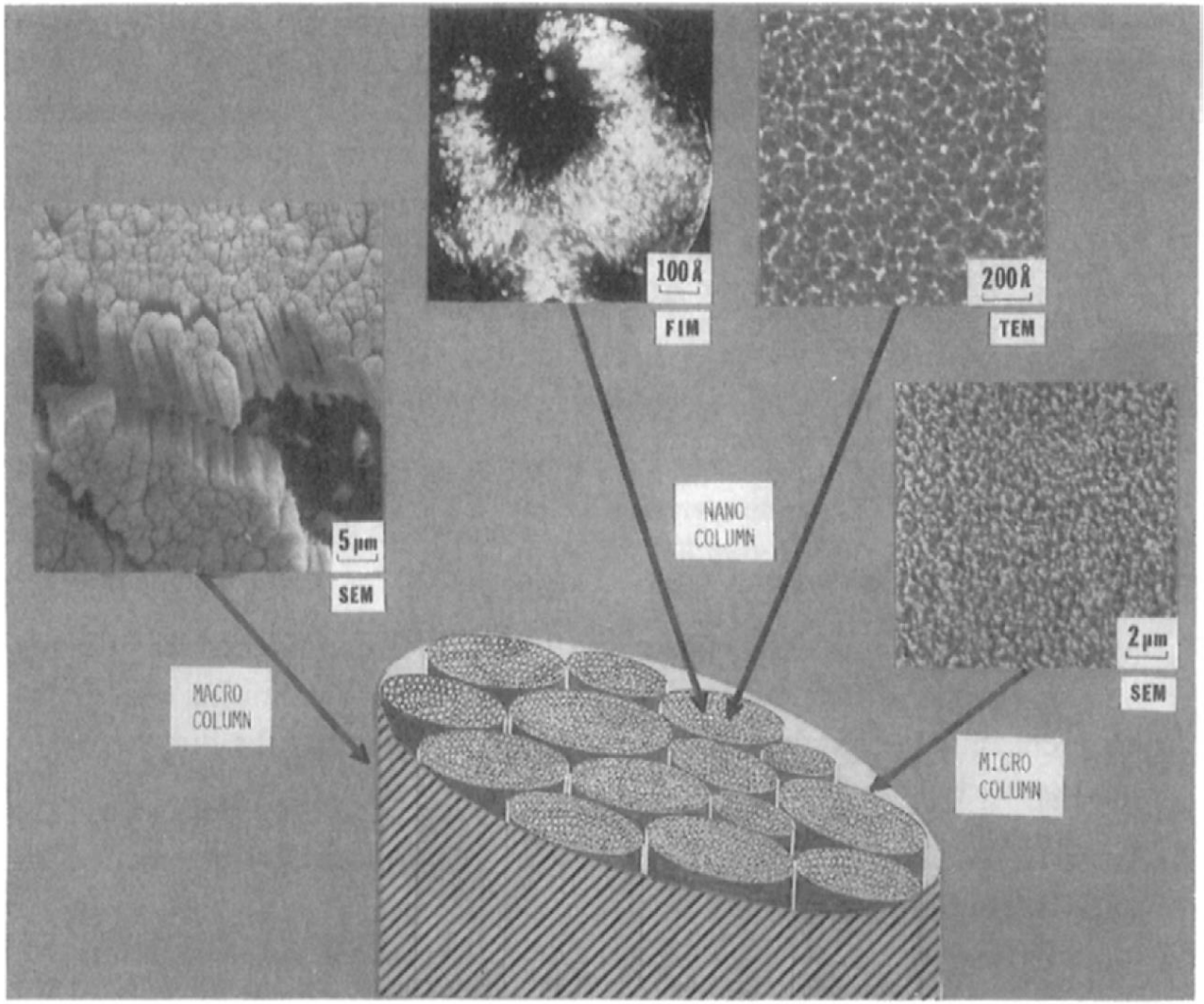

Figure 9-6 Schematic representation of macro-, micro-, and nanocolumns for sputtered amorphous Ge films. (From Ref. 8.)

Film density

Measurement of film density generally requires a simultaneous determination of both film **mass** per unit area and **thickness**.

experimental findings:

1) The density of both metal and dielectric films **increases with thickness** and reaches a plateau value which asymptotically approaches that of the bulk density. The gradient in film density is thought to be due to several causes, e.g., higher crystalline disorder, formation of oxides, greater trapping of vacancies and holes, pores produced by gas incorporation, and special growth modes which predominate in the early stages of film formation.

2) **Metal films tend to be denser** than dielectric films because of the larger void content in the latter.

3) Thin-film condensation is apparently accompanied by the incorporation of **large nonequilibrium concentrations of vacancies and micropores**. Whereas bulk metals may perhaps contain **a vacancy concentration of 10^{-3} at the melting point**, freshly formed thin films can have **excess concentrations of 10^{-2} at room temperature**.

4) In addition, microporosity on a scale much finer than imagined in zones 1 and T has been detected by transmission electron microscopy. **Voids measuring 1nm in size** have been revealed **in films prepared by evaporation**. Limited surface diffusion, micro-self-shadowing effects, and stabilization by adsorbed impurities encourage the formation of microporosity.

Film density

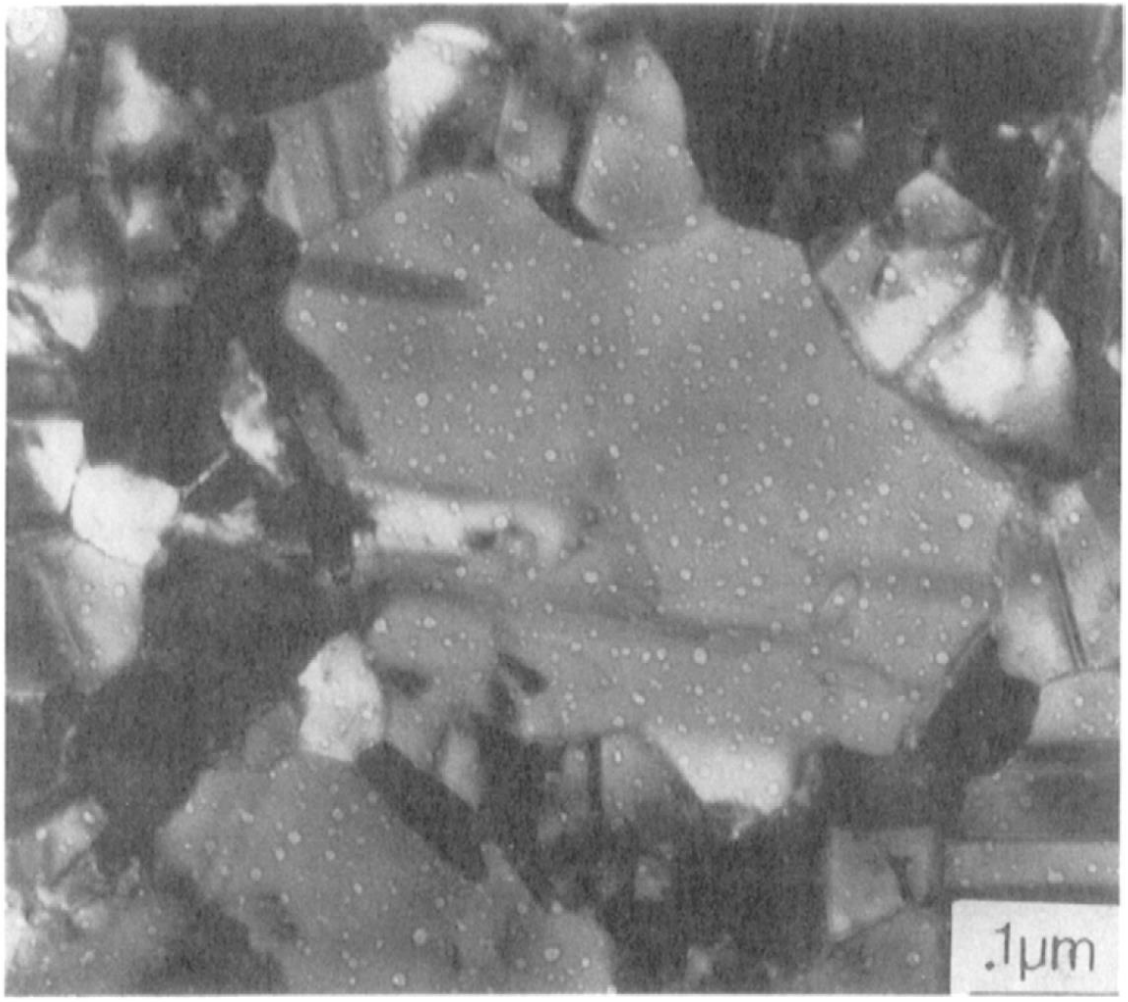

Figure 9-7 Transmission electron micrograph showing microvoid distribution in evaporated Au films. (Courtesy of S. Nakahara, AT&T Bell Laboratories.)

Computational simulations of film structure

Simulations have been performed to model vapor-phase deposition, epitaxial growth, ion-beam bombardment, and cluster-beam deposition.

In simulating these processes the major variables that must be accounted for are the energy, size, and composition of the depositing species, and the temperature and nature of the substrate.

The energy of the depositing species often establishes the division as to what will be modeled and how.

For low energies the equilibrium structural morphology and arrangement of atoms is evaluated through a combination of geometric and probabilistic considerations. The **Monte Carlo stochastic lattice-gas and solid-on-solid** simulations are of this type.

On the other hand, a **molecular dynamics approach** is used for modeling the effects of impinging particles having higher energy; here ultrashort-time kinetic interactions between the particle and surface as well as atomic displacements are often of interest.

Both kinds of simulations reflect the spirit of statistical mechanics because they attempt to model macroscopic behavior by summing over the collective dynamical behavior of large numbers of individual atoms.

Monte Carlo simulations of film structure

Most of the crystal growth studies to date have been carried out by **Monte Carlo or random "ballistic aggregation" simulations** which superimpose the statistics of atomic placement on a geometric array of surface sites.

In an intuitively simple simulation of film deposition, **individual hard spheres (atoms)** are serially "**evaporated" onto a growing film at a fixed angle**. The spheres are allowed to relax following impingement **into the nearest triangular cradle** formed by **three prior deposited atoms**, thus maximizing close atomic packing.

The simulation shows that **limited atomic mobility** during low-temperature deposition reproduces **film morphologies observed experimentally**. As examples, film density decreases with increasing α.

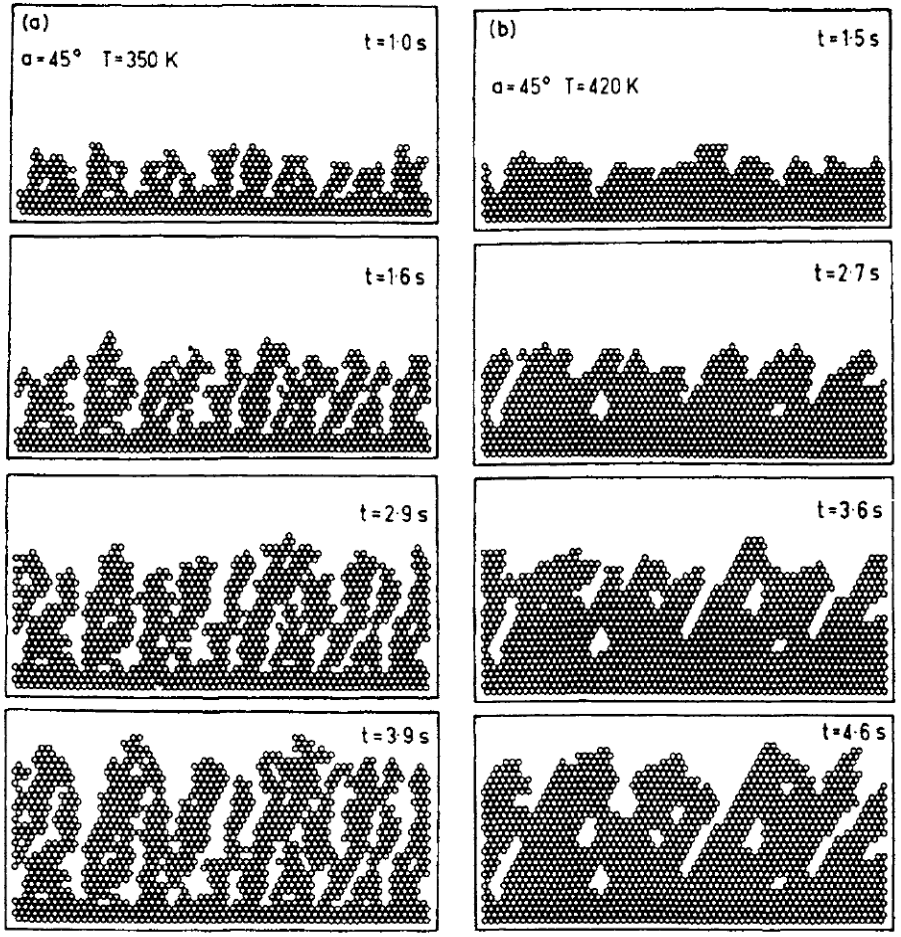

Figure 9-9 Computer-simulated microstructure of Ni film during deposition at different times for substrate temperatures of (a) 350 K and (b) 420 K. The angle of vapor deposition α is 45°. (After Ref. 20.)

Molecular dynamics simulations

In contrast to the Monte Carlo determinations of equilibrium structures, **molecular dynamics (MD)** simulations place a greater **emphasis on the motion and physical behavior of the involved atoms**.

An attempt is made in MD to distinguish between specific atomic species, i.e., metals and semiconductors, by employing a potential energy function (U(r)) that describes their pairwise interaction. The **two-body Lennard-Jones** potential, i.e.,.

$$U(r) = 4U_0[(a/r)^{12} - (a/r)^6],$$

is often chosen for the purpose since it displays an **attractive component (second term) when atoms are far apart**, but **strong repulsion (first term) when they approach too closely**. Terms U_0, a, and r represent the potential well depth, lattice dimension, and distance between atoms, respectively, and are selected to model the behavior of specific materials.

Molecular dynamics simulations

Molecular dynamics modeling is particularly instructive in depicting the otherwise **unobservable instant** when **an ion impacts a growing film**.

The structure shown illustrates an energetic **100 eV Ar ion impinging** on a rough Ni surface.

Atoms 1, 2, and 3 are of particular interest because the **overhang** they lie on would appear to enclose a void with further Ni atom deposition.

Within ~ 1 ps of impact these atoms sputter directionally in a way that enhances adatom surface diffusion.

After another ~ 10 ps a **further collision-cascade sequence** and **surface relaxation** ensue.

In the process the **protruding ledge disappears**, lessening the probability of entrapping another void and **the film densifies**

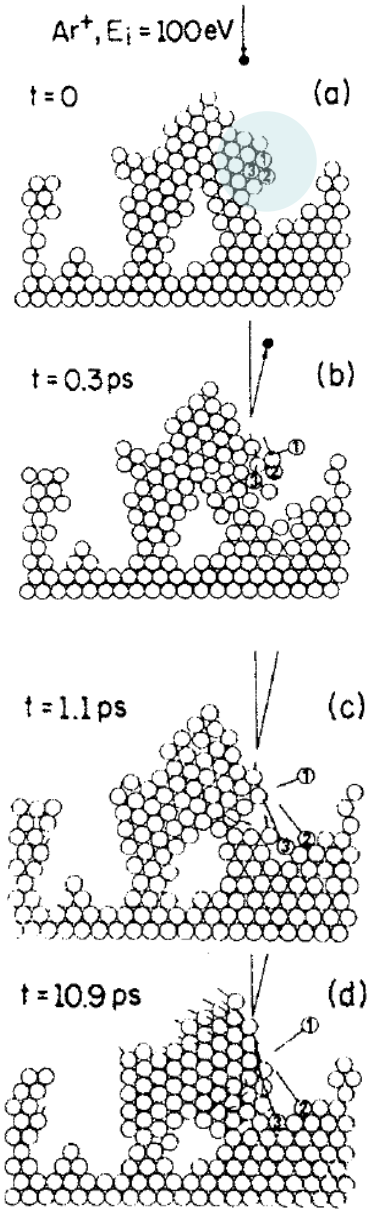

Ohring 2002

Grain growth I

We start with the widely known fact that when solids are heated, grains grow.

Assuming **grain boundary (GB) segments** have a **radius of curvature (R)**, the **velocity of boundary motion (v)** is related to the rate at which R changes with time t, or dR/dt.

But the boundary **moves when atoms hop across the interface between grains** in an effort to lower the GB free energy per unit area and the associated driving force is proportional to γ_{GB}/R to that $dR/dt \sim \gamma_{GB}/R$. Upon integration:

$$R^2 - R_0^2 \simeq kt^{1/2}$$

where R_o is the initial grain radius and k, which has absorbed γ_{GB}, is a thermally activated constant.

Parabolic grain-growth kinetics is thus predicted and usually observed in bulk solids. Importantly, grain growth is normal, which means that the shape of the grain size distribution function does not change with time.

Grain growth II

To simplify matters, we consider a film consisting of polygonal grains oriented as columns, i.e., grain boundaries normal to the substrate plane. Now free energies associated with the substrate interface and upper film surface play important roles.

This leads to the following predictions and experimental observations:

1. Normal grain growth is not expected in thin films. Instead, **abnormal grain growth is predicted**. This is often manifested by **a bimodal grain size distribution caused by secondary grain growth** in which **some grains may grow excessively large** (e.g., by a factor of ~ 10^2)

2. Abnormal grain growth leads to an **evolution in the average crystallographic orientations of grains**. The effects are more pronounced the thinner the film.

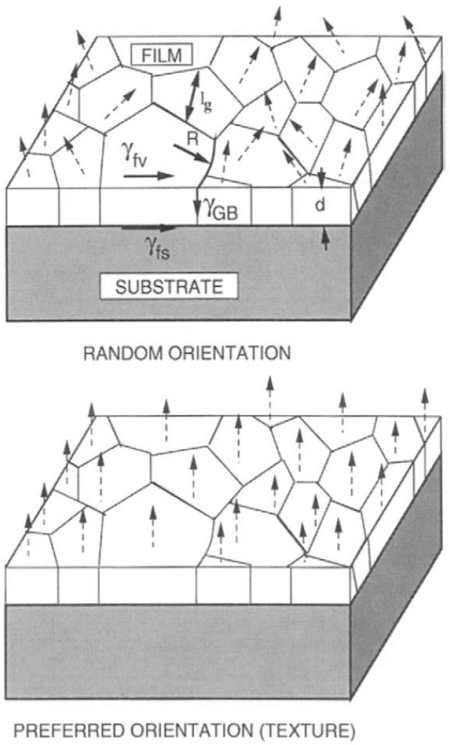

Figure 9-12 (Top) Model of a polycrystalline thin film consisting of randomly oriented polygonal grains. Surface energies associated with the substrate interface, grain boundary and upper film surface are shown. (After Ref. 30.) (Bottom) Same film displaying preferred orientation or texture. *Note:* Dashed arrows represent a measure of crystallographic orientation.

Grain growth III

3. At **elevated deposition temperatures** where low-strain growth occurs, surface and interfacial-energy minimization dominates grain growth. Under these conditions **close-packed surface textures evolve, e.g., (111) in FCC metals** and diamond-cubic elemental semiconductors.

4. **Grain growth** in films often **stagnates** when the grain size is **2 to 3 times the film thickness**. Surface **grooves** where grain boundaries meet the film surface are the **apparent cause of stagnation**.

Physically, boundary velocities go to zero when the driving forces for motion fall below critical levels. **Solute segregated at grain boundaries** often acts as a drag that inhibits growth.

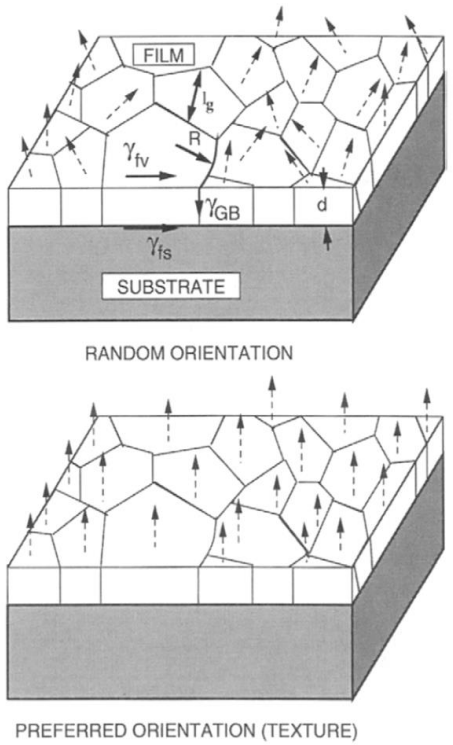

Figure 9-12 (Top) Model of a polycrystalline thin film consisting of randomly oriented polygonal grains. Surface energies associated with the substrate interface, grain boundary and upper film surface are shown. (After Ref. 30.) (Bottom) Same film displaying preferred orientation or texture. *Note:* Dashed arrows represent a measure of crystallographic orientation.

Energetics of grain growth

Potential **mechanisms of energy release** that can alter microstructure in thin films

1. Thermal energy: The available **thermal energy is simply k_BT** and in the range 20-400°C it varies between **25 and 58 meV/atom**.

2. Grain Growth: The energy released is the product of γ_{GB} and the area of eliminated boundaries.

3. Interface energy minimization. The (111) texture apparently stems from energy minimization at the film top surface and substrate interface.

4. Grain Growth coupled to solute precipitation. When grain boundaries sweep through grains that are supersaturated with respect to solute, precipitation is facilitated at the heterogeneous GB sites. This phenomenon is known as discontinuous precipitation.

As a **general rule**, energy release for mechanisms higher in the indicated order is capable of driving change for mechanisms lower in the order. Thus as an example **thermal energy release** and **solute precipitation** can both **trigger grain growth**.

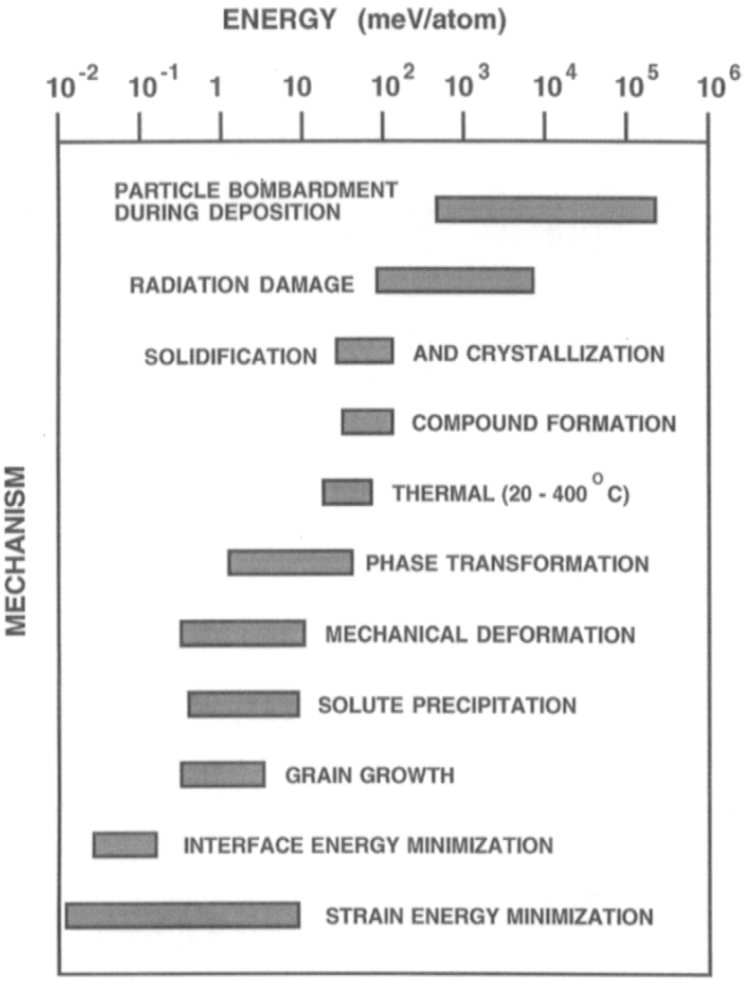

Figure 9-14 Sources of energy available to control thin-film microstructure. (After Ref. Courtesy of J. C. M. Harper, IBM, T. J. Watson Research Center.)

Texture I

Film texture is influenced by

deposition method and variables,
nature of the substrate,
energetic ion bombardment, and
geometrical confinement by surface features.

Diffraction, whether by **X-rays or electrons**, has been the traditional way to determine film crystallography and extent of texture. Thus, if a **disproportionate diffracted intensity** from a given (hkl) plane occurs **relative to its intensity in a powder sample of random grain orientations**, a preferred (hkl) texture exists.

Traditional definitions of texture have been expanded to **include misorientation between adjacent grains**; i.e., "grain-boundary texture".

We may thus imagine the involved grain boundaries separating grains that are tilted relative to one another. If both lattices are pinned at a common origin and the top lattice is rotated relative to the bottom one, certain lattice points will be shared or coincident at specific rotation angles. The two interpenetrating lattices form a **coincidence-site lattice or CSL** with a unit-cell volume some multiple of the original lattice unit-cell volume.

Texture II

Generallly manifestations of film **texture are quite varied** and **not easily predicted**.

In general, **evaporated films are more weakly textured** than sputtered films.

Texture **is barely discerned in metals deposited at very low temperatures (T/T_M <0.15)** where there is effectively no adatom mobility or grainboundary (GB) migration. At higher homologous temperatures **increased atom movements foster the development of texture**.

During growth: Sometimes, texture evolves from random in initial deposits, to strong orientation of low-energy planes parallel to the film surface, and finally, to changes in preferred texture as the film thickens further.

Thus **changes from (111) to (100) film orientation were observed in Ag films** after they reached a thickness of 2μm. Crystallographic twinning during film growth together with the changing competition between surface and strain energy all contribute to the observed texture and changes in it. Anisotropy of the elastic moduli will then favor the growth of low strain-energy oriented grains at the expense of those grains possessing higher strain energy.

Texture III

Substrate Effects: Both the substrate composition and roughness affect film texture.

Effect of Energetic Particle Bombardment: During sputtering, ion and neutral atoms bombard growing films under normal incidence and typically possess energies from fractions of an eV to upwards of 100 eV. Increasing target power and changes in the gas-discharge composition can strengthen the film texture or even change it.

Patterning Blanket Films: Even though we have been exclusively concerned with blanket films, the discussion also applies to patterned and geometrically confined films, but with modification. For example, originally sputtered Al-Cu films exhibit a strong (111) texture. In submicron-wide and -thick Al-Cu interconnections that are lithographically patterned from such films, a bamboo microstructure emerges.

Texture: XRD measurements

Texture : Preferred orientation
Preferred crystallographic orientation

Pole figure
Crystal symmetry/Specimen symmetry

Texture Component
{hkl}Plane <uvw>Direction

Rolling texture FCC
Copper component {112}<111>
(111) Pole figure

Recrystallization texture FCC
Cube component {100}<001>
(111) Pole figure

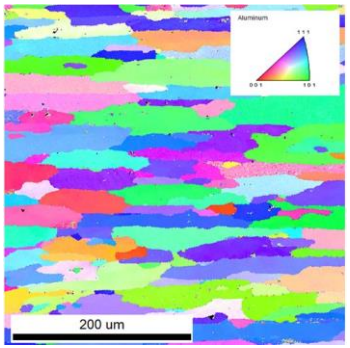

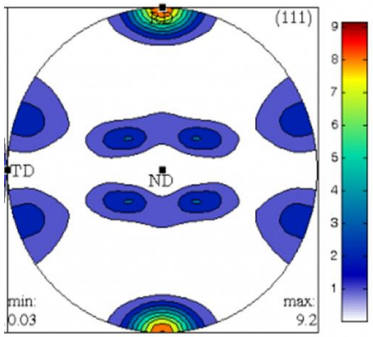

Annealing

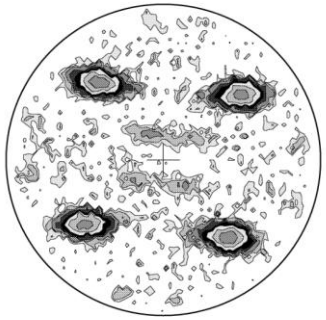

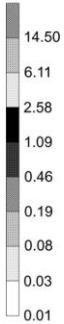

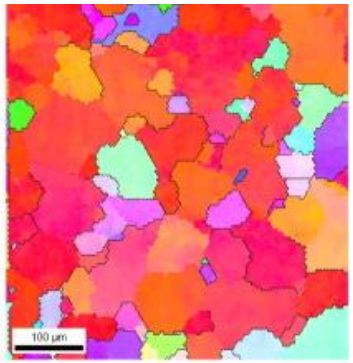

FIG. 6b

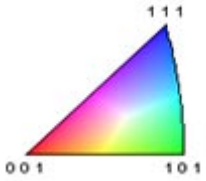

Key point: Texture in the bulk materials depends on the processing route/material history

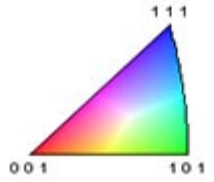

Measurement Setup : X-ray Pole figure

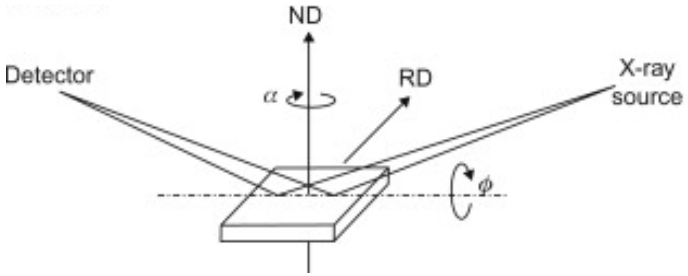

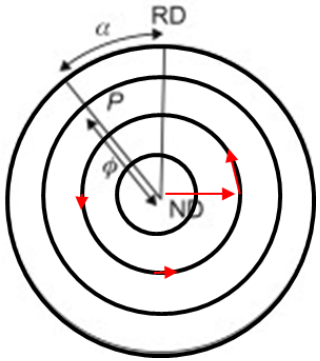

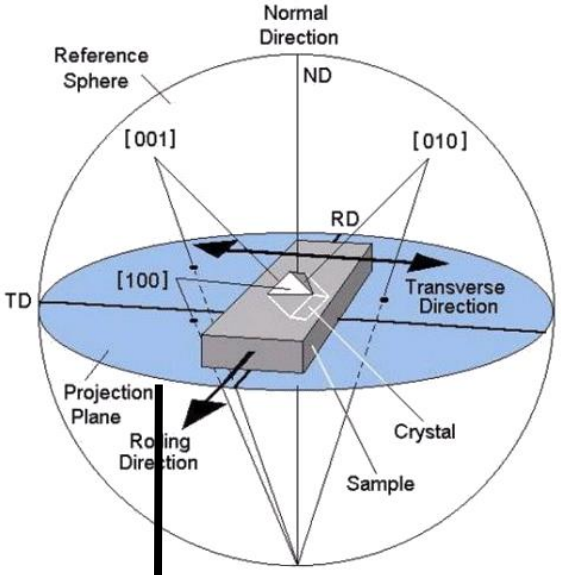

Fix incident and diffraction angle for Bragg condition

Ni (111) : θ: 22.0 and 2θ: 44.0
Tilt out of plane (Φ) and rotate the sample in plane (α) in steps

Measurement Setup

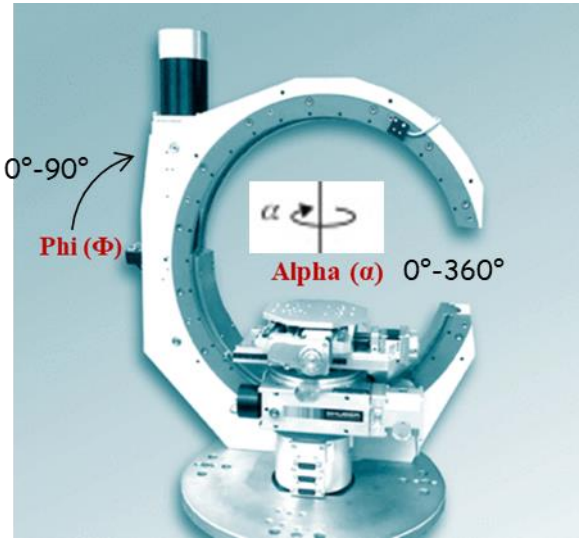

ND is parallel is (111) plane and (100) plane Projection is 54.7° from ND

Two dimesional projection plane

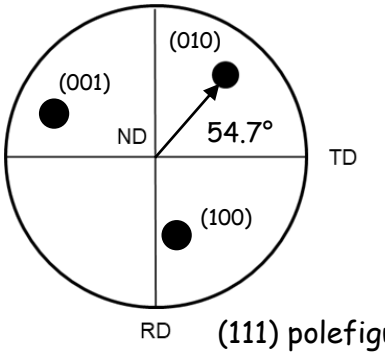

(111) polefigure

Texture: XRD measurements

- *Deposition rate* **(nucleation rate)**
- *Deposition temperature* **(ad-atom mobility)**
- *Choice of substrate* **(lattice mismatch and interface energy)**

1. Random texture films
(Room temperature deposited copper film)

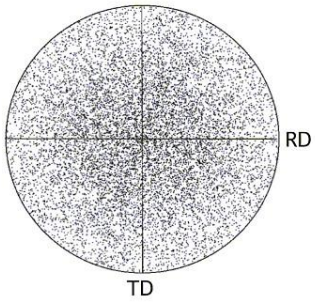

- Polycrystalline and amorphous films
- **No preferred orientation**

2. Fiber texture films
(Electrodeposited Nickel Film)

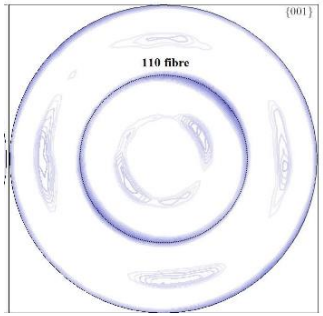

(100) pole figure

- Preferred **out of plane orientation**
- No in-plane alignment

3. Bi-Axial textured films
(Sputtered TiN film)

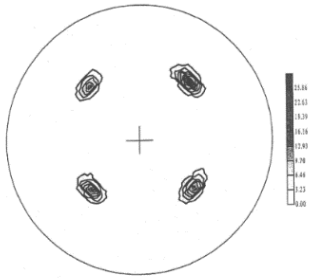

(100) pole figure

- **Preferred in plane as well as out of plane orientation**
- **Higher spreading** in the orientation and mosaicity

4. Epitaxial films
(Fe2O3 film /Al2O3)

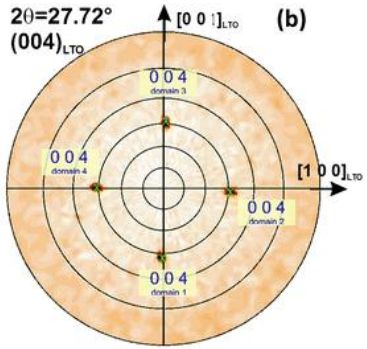

(012) pole figure

- Preferred **in plane as well as out of plane orientation**
- **Lower spreading** in the orientation and mosaicity

Texture in thin films

Alignments of Crystallites

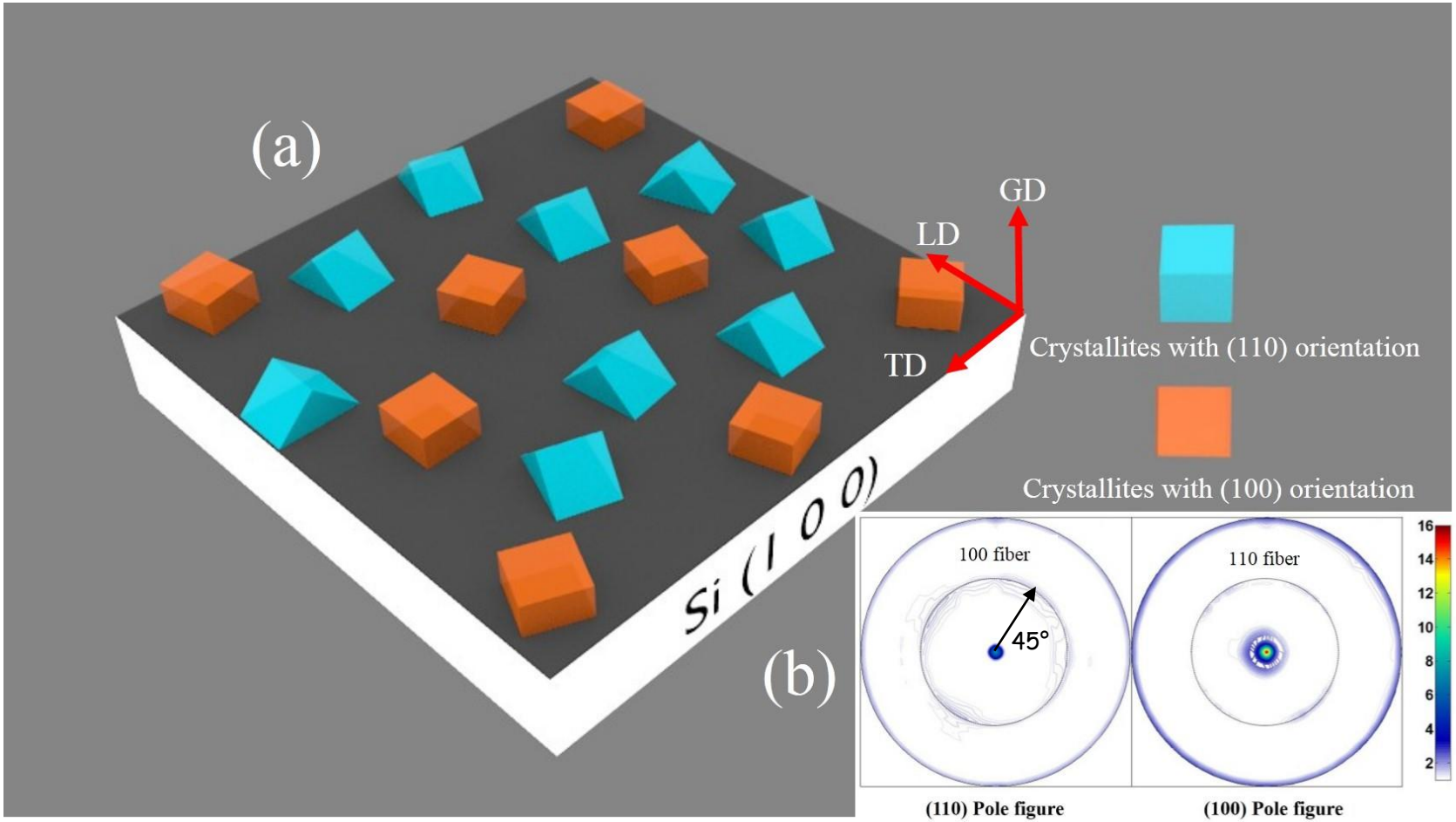

* Pole figure shows only out of plane alignments of columns

Stages of texture formation in thin films

Texture formation in thin films is basically dependent on the three parameters, namely:

1. Interfacial or surface energy
2. Grain boundary mobility
3. Strain energy difference between crystallographic variants

Texture formation in thin films takes place during the deposition processes. On annealing, the texture of the film further changes.

The formation of texture in thin films is influenced by following kinetic processes:

- Nucleation
- Pre-coalescence
- Coalescence
- Post-coalescence stage
- Post deposition annealing, which might involve recrystallization as well as grain growth.

Stages of texture formation in thin films

- **Nucleation:** Nucleation is considered as **orientation independent process,** particularly for the processes based on **physical vapour deposition**. It is important to note here that **oriented nucleation** is a possibility only when the critical nucleus size is not very small. However, in many deposition processes, the **vapour phase** is so much super-saturated that the nucleus size is very small. A typical calculation for the condition of sputter deposition of a FCC metal leads to a nucleus size **~0.1nm**. Obviously under such a situation, oriented nucleation is not a possibility.

- **Pre-coalescence:** In the process outlined above, a film forms through heterogeneous nucleation of particles which partially wet the substrate surface. Texture evolution at this stage depends on the involved surface and interface energies.

- **Coalescence:** As islands coalesce they can undergo accelerated coarsening processes with material exchange through self-diffusion on the particle surfaces, and through grain boundary motion. The term "**coarsening**" is used here to describe processes in which islands grow at the expense of other islands which have a higher energy per atom. In this case, particles with a high energy per atom will shrink while particles with a low energy per particle will grow. **In the late stage of coalescence, a few grains with (111) texture (FCC) typically grow to be very large**. As the film is further thickened the (111) texture becomes still more dominant

Texture in thin films

❖ **Post-coalescence stage: Microstructure dependent texture evolution**

$T_R = T(K)/T_M(K)$
High

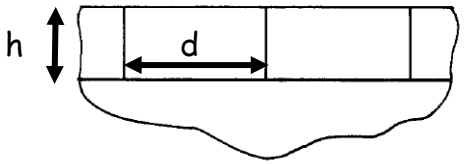

Equiaxed columnar grain structure

- **Grain size d is uniform through the thickness h of the film**
- **Grain size (d) ~ 2 * Film thickness (h)**
- **Grain growth dominated microstructure and texture**

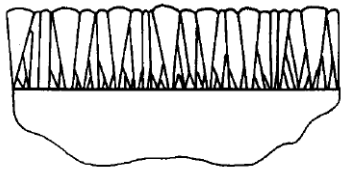

$T_R = T(K)/T_M(K)$
Low

Non-equiaxed columnar grain structure

- **Grain size is small at the film-substrate interface**
- Increases through the thickness of the film.
- **Growth rate anisotropy dominated microstructure**

Texture in thin films

- Post deposition annealing

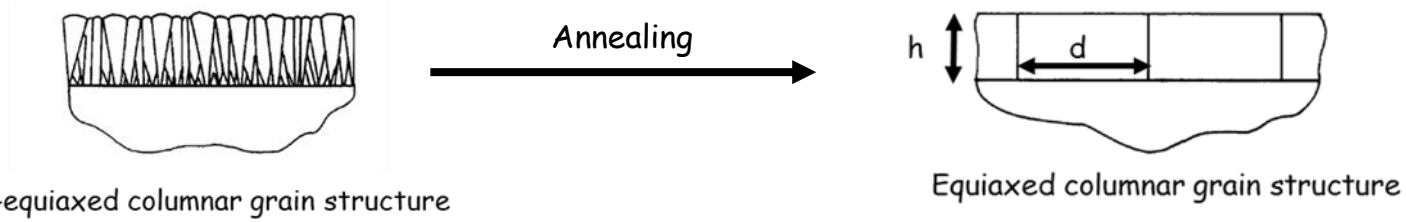

Grain growth during post-deposition annealing can lead to a surface and interface energy minimizing microstructure and texture.

Film and its substrate generally have **different thermal expansion coefficients**, differential thermal expansion during heating can lead to a **substantial biaxial strain in a film**.

Elastic anisotropy can therefore lead to high strain energy density differences for different grains. For a biaxial strain e, the difference in strain energy density for two grains is given by

$$\Delta W_\varepsilon = (M_1 - M_2)\varepsilon^2$$

Where M_1 and M_2 are effective biaxial moduli and depend on the crystallographic orientation of the grains with respect to the plane of the strain. For grains with (100) and (111) texture

$$M_{(100)} = C_{11} + C_{12} - \frac{2C_{12}^2}{C_{11}} \qquad M_{(111)} = C_{11} + C_{12} - \frac{C_{12}(C_{11} + 3C_{12} - 2C_{44})}{C_{11} + C_{12} + 2C_{44}}$$

sculptured films

The C- or S-shaped film was simply the result of continuously tilting the substrate relative to the evaporation source, first in one direction from 5° to 175° and then back again to 5°.

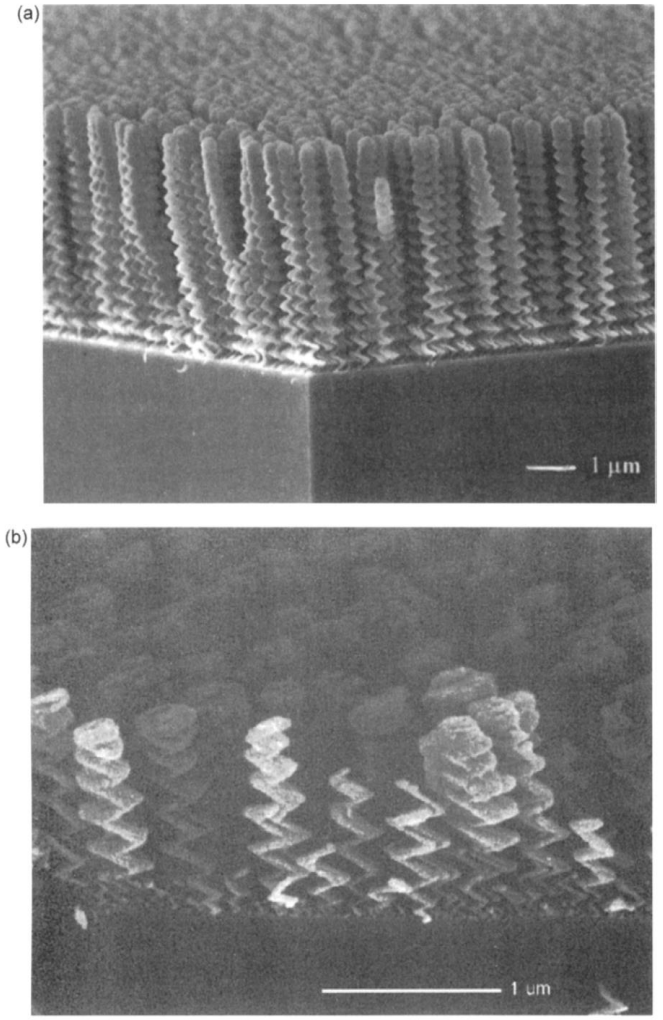

Figure 9-19 Sculptured film structures produced by an 85° oblique flux of evaporant. (a) Helical columns produced by rotary substrate motion. (b) Zigzag columns produced by alternating tilting. (From Ref. 51. Reprinted with the permission of the authors.)

Ohring 2002

Amorphous thin films

Amorphous metal alloys and virtually all elemental and compound semiconductors, semimetals, oxides, and chalcogenide (i.e., group VI-containing elements) glasses have been prepared by a variety of PVD and CVD techniques.

Topological short-range order is characterized by an average number of nearest neighbors or z, the coordination number, as well as by the mean separation of atoms. The radial distribution function (RDF), which can be determined by X-ray diffraction, provides values for z as well as nearest-neighbor distances. For example, in amorphous metal alloys and elemental semiconductors, z is 12 and 4, respectively.

Since they contain a huge number of different atomic configurations, amorphous solids are usually described in terms of statistical distribution models that fall into two categories, namely, **dense random (close) packing (DRP)** and **continuous-random-network (CRN).** The DRP model is better suited to amorphous alloys, whereas amorphous elemental semiconductors are more closely described in CRN terms.

Amorphous SiN and SiO_2

Silicon nitride is normally prepared by CVD and reacting silane with ammonia in an argon plasma, but an N_2/SiH_4 discharge can also be used. Like a-Si, amorphous silicon nitride is overconstrained because there are four bonding electrons on Si and three on N.

During plasma deposition however, as much as 30 at.% hydrogen can be incorporated, and by terminating Si and N bonds the overconstraint is relieved. It is in this sense that silicon nitride is often described as a ternary solid-solution alloy, SiNH.

In contrast, plasmadeposited SiO_2 films contain very little hydrogen. Because divalent oxygen atoms can readily locate silicon atoms within the amorphous network, there is little overconstraint. Uncompensated oxygen bonds are terminated by hydrogen, leaving a relatively small concentration of OH groups behind.

summary

- Although greater directionality of atom transport occurs in sputtering and evaporation than in CVD processing, films from all three methods share common zone structures and morphological features.
- SZM rely on four basic processes: shadowing, surface diffusion, bulk diffusion, desorption, the latter three scale with the homologeous T
- Zone 1: cone-like, voided boundaries due to limited adatom mobility at T_S/T_M <0.3 and shadowing
- Zone 2: columnar, tight boundaries due to surface and grain-boundary diffusion at 0.3 < TS/TM < 0.50
- Zone 3: Equiaxed due to bulk diffusion for (T_S/T_M > 0.5).
- SZM pressure effect: reduction increases density, increase more open grain morphology
- SZM T effect: At elevated temperatures both surface and bulk diffusion allow atoms to access equilibrium lattice sites, fill voids, and enlarge grains.
- SZM ion bombardment: increase adatom motion same as T
- Grain morphology: Shadowing effects, substrate temperature, and energy of depositing atoms are the influential factors that affect grain morphology. Columns are observed on both crystalline and amorphous substrates, and in crystalline as well as amorphous films. Nested columns in thick films
- Tangent rule: columns oriented towards source, $\tan\alpha = 2\tan\beta$
- Film density: needs mass and thickness measured, increases with thickness, metals denser than dielectrics, up to 1% vacancies in films, 1nm sized voids in evaporated films
- Monte-Carlo & MD simulations revealed mechanisms of zone I growth
- Parabolic grain growth follows $R^2 - R_0^2 \simeq kt^{1/2}$, abnormal grain growth also common, grain growth stagnates often at 2-3x film thickness, interfacial energy minimization dominates at high T and (111) surface texture establishes, grain growth can be driven by processes that relieve more energy than grain growth needs such as precipitation or strain energy.

summary

- Texture is orientation of grains and misorientation between grains, pole figures display texture, no texture in zone 1, texture evolves during growth due to optimization of surface and strain energies, and is influences by substrate (epitaxy), ion bombardment and surface pattern.
- Deposition of sculptured film is possible exploiting the tangent rule via substrate rotations.
- Amorphous thin films are deposited typically in zone 1, characterized by RDF from XRD,
- amorphous SiN and SiO_2 include H

exercises

- Name the four most important mechanisms responsible for film microstructure
- What are the temperature ranges for zone I, zone II and zone III
- What are the effects of process pressure, temperature in the structure of sputtered film?
- How does the substrate bias influence structure of a sputtered film?
- Give 3 arguments why SZM from evaporation differs from sputtering?
- If the flux of evaporating atoms is directed at an angle 45° to the normal to the substrate, assuming the tangent rule, determine the direction of growth of the columnar growth in the thin films.
- Differs film density from the density of the corresponding bulk materials?
- Discuss grain size in thin films based on deposition T and as a function of film thickness
- Name 2 processes that can drive grain growth after deposition
- Discuss texture in thin films based on surface energies and residual stress. Include the effect of film thickness.
- Name typical materials of amorphous thin films

Ohring 2002